Mechanisms of High-Order Perturbative Photoemission from Cu(001)

F. Bisio,[1,2] M. Nývlt,[1,3,*] J. Franta,[1,3] H. Petek,[4] and J. Kirschner[1]

[1]*Max-Planck Institut für Mikrostrukturphysik, Weinberg 2, D-06120 Halle (Saale), Germany*
[2]*CNR-INFM, Unità di Genova, via Dodecaneso 33, I-16146 Genova, Italy*
[3]*Faculty of Mathematics and Physics, Institute of Physics, Charles University, Ke Karlovu 5, CZ-12116 Praha 2, Czech Republic*
[4]*Department of Physics and Astronomy, University of Pittsburgh, Pittsburgh, Pennsylvania 15260, USA*

(Received 1 July 2005; published 27 February 2006)

We observed high-order 2- to 4-photon photoemission and above threshold photoemission (ATP) processes with 3.07 eV light from the Cu(001) surface. The intensity of 3-photon photoemission via excitation through the $n = 1$ image potential state significantly exceeded that of the 2-photon process. The ATP occurs either via single photon transitions from the image potential resonances above the vacuum level or by multiphoton transitions from image potential states below the vacuum level. The experimental ratio of the m- to $(m + 1)$-photon process yields is sensitive to the electronic band structure of the solid.

DOI: 10.1103/PhysRevLett.96.087601 PACS numbers: 79.60.−i, 73.20.−r, 82.50.Pt

The nonlinear photoemission induced by ultrashort laser pulses has become one of the most powerful techniques for the study of the electronic excitations in matter. Time-resolved two-photon photoemission (2PPE) has contributed greatly to the understanding of the ultrafast electron dynamics at solid surfaces [1–7], and is now starting to be quantitatively understood in terms of the known band structure of metals [7].

By contrast, higher-order multiphoton photoemission processes in solids, which can extend the energy range of the studied unoccupied states and provide further information on photoexcitation processes, have received only little attention. This is mainly because their observation requires very intense optical fields and their considerably reduced photoelectron yields can be overwhelmed by space charge effects from the lower-order processes [2,4,8–11]. Moreover, nonphotoelectric effect emission through the surface plasmon excitation and possibly tunneling, leading to ponderomotive acceleration of photoelectrons up to 0.4 keV energy [10,12], has been reported with lower external fields than employed in our work. Therefore, the mechanisms for high-order photoelectric excitations at solid surfaces, in particular, to what extent they are governed by the band structure of metals, are essentially unknown. Especially, the mechanism underlying the above threshold photoemission (ATP) effect in solids [8–10,13], a process in which the penultimate state of a multiphoton transition is above the vacuum level, is not clear yet.

In this Letter we report the observation of multiphoton photoemission processes from Cu(001) surfaces up to the fourth order in light intensity that involve ATP. We have observed a third-order process whose yield significantly exceeds that of the second-order process, which has not been observed so far for metals. We account for this anomalous increase of the third-order photoelectron yield in terms of a previously unknown two-photon resonance between the bulk d bands and $n = 1$ image potential (IP) state, which should also occur in other transition and noble metals. We also demonstrate that the ATP proceeds either via resonant or nonresonant excitation pathways with significantly different efficiencies. The resonant ATP is ascribed to a lifetime of electrons excited to IP states above the vacuum level that is comparable or longer than the pulse duration.

The photoemission experiments were carried out in an ultrahigh vacuum system (pressure $<7 \times 10^{-11}$ mbar). A self-built Ti:sapphire oscillator provided the frequency-doubled pulses with the central energy of $\hbar\omega = 3.07$ eV, the band width of ~ 0.17 eV, the pulse length at the surface of <18 fs, and the pulse energy of ~ 1 nJ. The laser beam was focused on the surface to a spot of ≈ 40 μm in diameter. The incident peak power was below 10^{10} W/cm^2, corresponding to an electric field in vacuum $<3 \times 10^6$ V/m. The photoemitted electrons were analyzed by a cylindrical sector analyzer with parallel momentum ($k_{\|}$) resolution below ± 0.07 Å^{-1}. The Cu crystal was biased at -1 V. The angle between the incident beam and the axis of the analyzer was fixed at 35° (inset of Fig. 1), while the sample could be rotated to provide a range of electron detection angles with respect to the surface normal of $-35°$ to 45°. A clean and ordered Cu(001) surface was prepared by standard sputtering and annealing procedures. Surface regions with rough spots giving rise to anomalously high electron yields were avoided. The optical and the electron emission plane was aligned parallel either to the [100] or the [110] axis. All the experiments were carried out at 300 K.

In Fig. 1 we plot the photoelectron yield along the surface normal for p-polarized (p_{in}) and s-polarized (s_{in}) incident radiation. The final state energy of the electrons is taken with respect to the Fermi energy E_F. The 2PPE to 4PPE spectral regions are indicated. In Fig. 2 we plot the angle-resolved spectra measured with p_{in} and s_{in} light. The electronic state dispersions extracted from the data are summarized in Fig. 3.

Whenever high excitation fields are employed, the occurrence of nonphotoelectric electron emission, such as

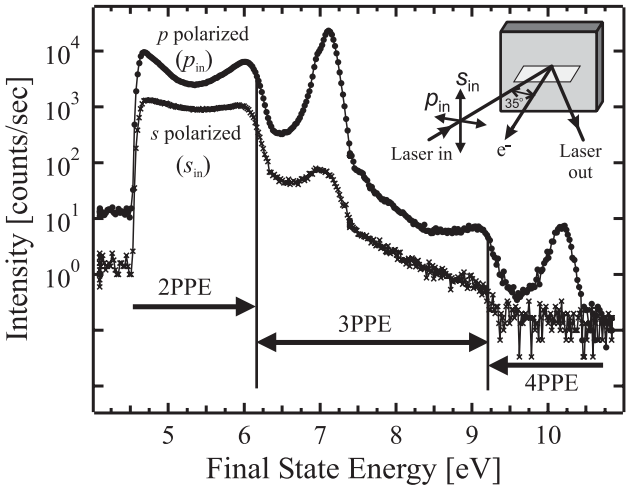

FIG. 1. Normal emission multiphoton photoelectron yield from the Cu(001) surface excited by p_{in} and s_{in} radiation. Notice the logarithmic scale. The inset depicts the normal emission experimental geometry.

tunneling, plasmon mediated emission, or thermionic emission [10,12], must be carefully considered. These alternative photoelectron generation processes, which are insensitive to the band structure of metals, give rise only to structureless spectra. However, our spectra clearly display well-resolved features up to the maximum energy of interest, which we can assign unambiguously to the surface and bulk bands of Cu. In addition, the photoelectron yield in the 2–4PPE regions follows the I^m power dependence appropriate for each order. Consequently, the photoelectric effect gives the dominant contribution to our spectra, which can be interpreted on the basis of band structure effects.

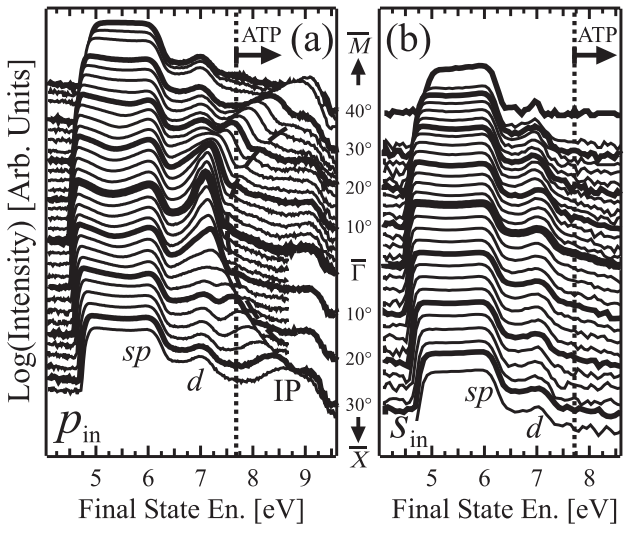

FIG. 2. Angle-resolved multiphoton photoelectron yield measured along the $\overline{\Gamma M}$ ([100]) and $\overline{\Gamma X}$ ([110]) directions of the surface Brillouin zone for (a) p_{in} and (b) s_{in} incident radiation. The dotted line represents the energy threshold for ATP processes.

Multiphoton transitions can proceed either directly through multiphoton absorption via real or virtual intermediate states above E_F, or indirectly through the population of real intermediate states involving energy and/or momentum scattering [3,5,7].

The assignment of the various features of our spectra is performed referring to Fig. 3, where the electronic structure of the Cu(001) surface at $\overline{\Gamma}$ (right panel) and along the $\overline{\Gamma M}$ and $\overline{\Gamma X}$ lines (left panel) is reported. We focus on the resonantly enhanced multiphoton processes above the second order and on transitions involving ATP.

Within the 3PPE region, a very intense peak appears in the p_{in} normal emission spectrum at the final state energy of 7.1 eV (Figs. 1 and 3). Its intensity is so high to exceed in magnitude all the measurable 2PPE features, obviously contradicting the expected decrease of the electron yield for an increasing order of nonlinearity. By contrast, the 3PPE intensities above 7.5 eV are reduced by approximately 2 to 3 orders of magnitude with respect to their 2PPE counterparts. This suggests the occurrence, limited to p_{in} excitation, of a multiphoton resonantly enhanced transition. According to the band structure of Fig. 3, a doubly resonant multiphoton transition is indeed possible for $\hbar\omega = 3.07$ eV at $\overline{\Gamma}$ (dashed lines in the right panel of Fig. 3). In the first step, electrons are excited resonantly from the occupied d band either to the unoccupied sp band or to the $n = 0$ surface resonance (SR); in the second step, resonant excitation populates the IP $n = 1$ state at 4.03 eV above E_F; and in the final step, electrons are photoemitted at 7.1 eV energy. Our data show that the double resonance from the top of the d bands is the primary factor that determines the giant 3PPE p_{in} yield at 7.1 eV, while its suppression causes the 3PPE to drop below the average 2PPE intensity. For instance, the much weaker peak at 7.0 eV in the s_{in} spectrum shares the same resonant d-sp interband transition as the p_{in} peak; however, due to a matrix element effect [1], the only $k_{\|}$ conserving transition from the intermediate sp band to the photoemitted state is a nonresonant two-photon process. Hence the 3PPE yield at 7 eV for s_{in} is smaller than the corresponding p_{in} yield by a factor of at least 10^2. Similarly at larger $k_{\|}$, the parabolic dispersion detunes the IP $n = 1$ state from the nondispersing d-sp transition. The transitions from d, sp, and via $n = 1$ IP state give separate contributions to the p_{in} spectra (Fig. 2), with low yields. The double d-sp-IP resonance gives the opportunity to observe the population of the IP state from a specific point of the d bands, which is highly localized in the reciprocal space. Such doubly resonant excitations from specific points in the d bands to IP states should occur in all transition and noble metals, although they may require commonly employed two-color excitation techniques. Such resonances can be used to probe magnetic interactions through spin polarized IP states [14].

We now focus on the ATP effect, occurring whenever the final state energy is larger than $E_V + \hbar\omega \approx 7.7$ eV

($E_V = 4.63$ eV is the sample work function at $\overline{\Gamma}$). Our data clearly exhibit two classes of ATP transitions.

The first class includes the ATP transitions involving the $n = 1$ and the $n = 2$ IP states above E_V. The IP $n = 1$ and 2 states disperse with characteristic free-electron-like parabolas, with effective masses $m_1^* = (0.94 \pm 0.1)m_e$ and $m_2^* = (0.84 \pm 0.2)m_e$ (dashed line in Fig. 2), in agreement with the literature [15]. For $k_\parallel > 0.4$ and 0.2 Å^{-1}, the IP $n = 1$ and 2 states, respectively, are found at energies above E_V (Fig. 3). Our data show that the ATP takes place when an IP state populated above E_V acts as the penultimate level in the multiphoton photoemission process. The vertical solid lines in the left panel of Fig. 3 depict an example of such an ATP transition via the $n = 2$ IP state. The occurrence of IP states above E_V for clean surfaces for large $k_\parallel$, long predicted theoretically [16] and confirmed here, is a consequence of the kinetic energy of the motion parallel to the surface not being available to do work against the image potential. This observation has important consequences, because resonant ATP requires an electron to reside at the surface above E_V for a sufficiently long time to absorb a further photon. The estimated inelastic scattering lifetime of an $n = 1$ IP electron at $k_\parallel > 0.4$ Å^{-1} is reduced from $\tau = 35 \pm 6$ fs at $\overline{\Gamma}$, [15] by electronic friction to $\tau \approx 15$ fs [6,17]. Thus, we can infer that the escape into vacuum or decay into the bulk of electrons excited to IP states with high $k_\parallel$ takes place on time scales at least comparable to our pulse duration. The excitation to IP states above E_V corresponds to the total internal reflection of electrons at the metal-vacuum interface at the critical angle. The conservation of $k_\parallel$ in photoemission is not only responsible for the existence of metastable states with high $k_\parallel$ above E_V, but it also explains the dispersion of the work function edge in Fig. 2 [18].

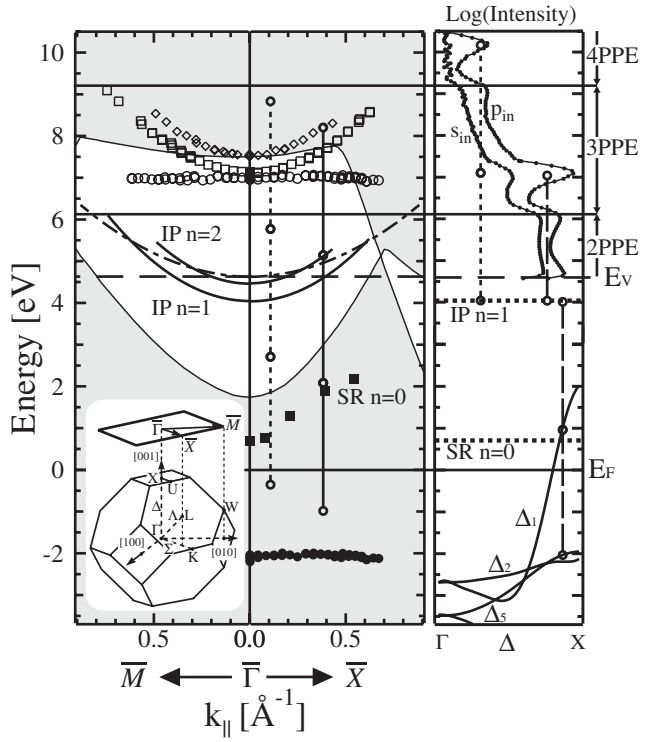

FIG. 3. Right panel: Calculated electronic band structure along the ΓX line (after Ref. [21]) and surface states at $\overline{\Gamma}$, pertinent to the normal emission geometry. Left panel: Surface projected bulk band structure (shaded area), vacuum level at $\overline{\Gamma}$, E_V (dashed line), threshold energy for the electron escape into vacuum (dash-dotted line) [18], and IP $n = 1$ and $n = 2$ states (solid lines). The peaks measured in angle-resolved photoemission are plotted by the open symbols. Circles, squares, and diamonds represent, respectively, the d band and the $n = 1$ and the $n = 2$ IP contribution. Initial d-band states are displayed as solid circles. Solid squares represent the $n = 0$ SR [22]. Selected laser-induced transitions are indicated by the vertical lines. The open circles at line termini represent the spectral width of the excitation pulses. The inset depicts the bulk and surface Brillouin zones.

The second class of ATP includes the ''conventional'' processes that are typically interpreted in terms of multiphoton transitions from states below E_V (e.g., the dotted lines in the left and the right panel of Fig. 3) [9,13]. An example is the 10.2 eV 4PPE peak in the p_{in} spectrum at $E = 7.1$ eV $+ \hbar\omega$, which is a replica of the IP $n = 1$ peak in 3PPE at 7.1 eV excited by two-photon nonresonant transition from the IP $n = 1$ state.

In the case of conventional ATP, the ratio R of the m- to the $(m + 1)$-photon process yields is often used to compare experiment and theory. For this purpose, the ratio R is often assumed to be independent of the photoemission transition moments [13]. However, our data show that the ratio of the 2PPE and 3PPE normal emission p_{in} yields in the energy region below the respective Fermi edges is a rapidly varying function of the final state energy [Fig. 4(a)]. In particular, R is approximately constant ($R \approx 350$) for the states located more than ~1 eV below E_F, but close to E_F, it increases up to $R \approx 10^3$ due to a pronounced peak in the

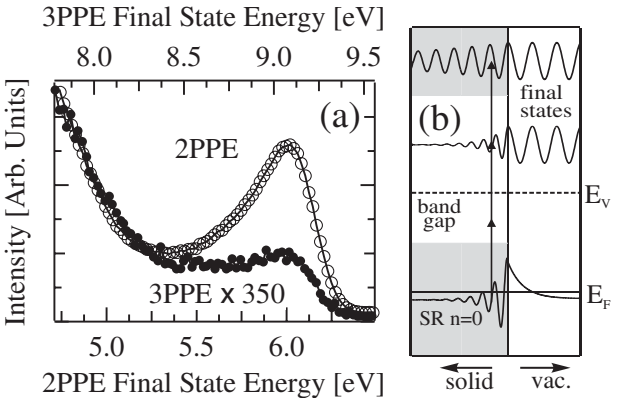

FIG. 4. (a) 2PPE and 3PPE Fermi edge regions measured in the normal emission geometry with p-polarized excitation. (b) Schematic diagram of the photoemission mechanism from the $n = 0$ SR into evanescent or propagating bulk final states.

2PPE signal. For the p_{in} polarization, this difference between the 2PPE and 3PPE spectra cannot originate from a dipole-selection-rule effect [19], but is due to a photoemission final state effect. The 2PPE peak has been ascribed to a low-energy tail of the unoccupied $n = 0$ SR that extends below E_F [4]. Since the 2PPE takes place via a final free-electron state lying in the bulk-projected band gap whose penetration in the bulk is evanescent [Fig. 4(b)], the surface localized $n = 0$ SR has a relatively large transition moment in comparison with the bulk Bloch states, which are delocalized within the solid [20]. By contrast, the corresponding final states for 3PPE lie within the projected bulk continuum [shaded area in Fig. 4(b)], and therefore have larger penetration into the solid. Under these conditions, the bulk states have a larger transition moment for 3PPE with respect to the corresponding 2PPE process, and the relative weight of the $n = 0$ SR state in the photoemission spectrum decreases. Therefore, the experimental value of R near the E_F edge for 3PPE and 2PPE is heavily affected by the transition moments. Such distortions of the $m/(m + 1)$-photon process yields can generally be expected for initial states with both surface and bulk character.

A more unambiguous way to extract R, which circumvents such transition moment effects, is to compare the intensity ratio of one- and two-photon excitations from the populated $n = 1$ IP state at 7.1 and 10.2 eV. In this case, $R = 2.5 \times 10^3$ is free of distortions due to the transition moment, because the $n = 1$ IP state is localized outside the surface. Its value is therefore a meaningful input for theoretical models of multiphoton processes. Moreover, the $n = 1$ IP state, which exists near the vacuum level of solids, should serve as a sensitive probe for the onset of tunneling through the image potential in the nonperturbative multiphoton photoemission regime.

The multiphoton processes that we report for the Cu(001) surface should be common to other low index surfaces of copper and other transition and noble metals provided that the excitation photon energies and k-space selection in electron analysis match the appropriate resonance conditions. Taking advantage of the weak dispersion of initial states common to the d bands, the resonance with dispersing sp or IP intermediate states can be provided by tuning $k_\parallel$. The ATP for IP states at $k_\parallel = 0$ and for metastable IP states at high $k_\parallel$ should be general since IP states and resonances are common to all metallic surfaces. The Cu(001) surface is particularly well suited for the observation of such effects due to the favorable energy of its resonances and the relatively long lifetime of its IP states.

In conclusion, we have investigated the mechanisms for multiphoton photoemission processes in the perturbative regime. Our results show that the three-photon excitation efficiency can exceed that of the two-photon process when favorable resonances exist at solid surfaces. We have also demonstrated the existence of the predicted IP resonances with a finite lifetime above the vacuum level of metals, which can enhance ATP emission. Our results point out the relevance of the band structure in the correct evaluation of the nonlinear photoemission yield from solids.

H. P. thanks M. N. and J. K. for their hospitality and the Alexander von Humboldt Foundation and NSF Grant No. CHE-0209706 for financial support. F. B. acknowledges support from MIUR-FIRB Program No. RBNE017XSW. M. N. thanks MSM 0021620834 research plan of the Czech Ministry of Education for financial support. The authors thank Neville Smith and Thomas Fauster for the insightful discussion of the parallel momentum dependence of the effective work function of metals, and Mrs. Heike Menge for preparation of high quality Cu(001) surfaces.

*Electronic address: nyvlt@karlov.mff.cuni.cz

[1] K. Giesen, F. Hage, F. J. Himpsel, H. J. Riess, and W. Steinmann, Phys. Rev. Lett. **55**, 300 (1985).
[2] R. W. Schoenlein, J. G. Fujimoto, G. L. Eesley, and T. W. Capehart, Phys. Rev. Lett. **61**, 2596 (1988).
[3] T. Hertel, E. Knoesel, M. Wolf, and G. Ertl, Phys. Rev. Lett. **76**, 535 (1996).
[4] S. Ogawa and H. Petek, Surf. Sci. **363**, 313 (1996).
[5] H. Petek and S. Ogawa, Prog. Surf. Sci. **56**, 239 (1997).
[6] W. Berthold *et al.*, Phys. Rev. Lett. **88**, 056805 (2002).
[7] N. Pontius, V. Sametoglu, and H. Petek, Phys. Rev. B **72**, 115105 (2005).
[8] S. Luan, R. Hippler, H. Schwier, and H. O. Lutz, Europhys. Lett. **9**, 489 (1989).
[9] W. S. Fann, R. Storz, and J. Bokor, Phys. Rev. B **44**, R10980 (1991).
[10] S. E. Irvine, A. Dechant, and A. Y. Elezzabi, Phys. Rev. Lett. **93**, 184801 (2004).
[11] I. Kinoshita, T. Anazawa, and Y. Matsumoto, Chem. Phys. Lett. **259**, 445 (1996).
[12] J. Kupersztych, P. Monchicourt, and M. Raynaud, Phys. Rev. Lett. **86**, 5180 (2001).
[13] F. Banfi *et al.*, Phys. Rev. Lett. **94**, 037601 (2005).
[14] A. B. Schmidt, M. Pickel, M. Wiemhöfer, M. Donath, and M. Weinelt, Phys. Rev. Lett. **95**, 107402 (2005).
[15] M. Weinelt, J. Phys. Condens. Matter **14**, R1099 (2002).
[16] J. Bausells and P. M. Echenique, Phys. Rev. B **33**, R1471 (1986).
[17] S. Garrett-Roe *et al.*, J. Phys. Chem. B **109**, 20 370 (2005).
[18] *Photoemission in Solids*, edited by M. Cardona and L. Ley (Springer-Verlag, Berlin, 1978), Chap. 1.
[19] J. Hermanson, Solid State Commun. **22**, 9 (1977).
[20] S. Hüfner, *Photoelectron Spectroscopy* (Springer-Verlag, Berlin, 1995), Chap. 6.
[21] G. A. Burdick, Phys. Rev. **129**, 138 (1963).
[22] S. L. Hulbert, P. D. Johnson, M. Weinert, and R. F. Garrett, Phys. Rev. B **33**, 760 (1986).